Scientific Research Publishing

Advances in Materials Physics and Chemistry, 2026, 16(8), 281-291
https://www.scirp.org/journal/ampc
ISSN Online: 2162-5328
ISSN Print: 2162-531X

Investigation and Modeling of the Photovoltaic Properties of Lead-Free $CsSn_{0.50}Ge_{0.50}I_3$ Perovskite Solar Cells

Saliou Seck, Alioune Sow, Mamadou Salif Mane, Modou Faye, El Hadji Mamadou Keita, Amadou Ndiaye, Bachirou Ndiaye, Babacar Mbow, Cheikh Sene

Department of Physics, Cheikh Anta Diop University, Dakar, Senegal
Email: saliou12.seck@ucad.edu.sn

How to cite this paper: Seck, S., Sow, A., Mane, M.S., Faye, M., Keita, E.H.M., Ndiaye, A., Ndiaye, B., Mbow, B. and Sene, C. (2026) Investigation and Modeling of the Photovoltaic Properties of Lead-Free $CsSn_{0.50}Ge_{0.50}I_3$ Perovskite Solar Cells. *Advances in Materials Physics and Chemistry*, **16**, 281-291.
https://doi.org/10.4236/ampc.2026.168016

Received: July 3, 2026
Accepted: August 3, 2026
Published: August 6, 2026

Abstract

In this work, a modeling study of $CsSn_{0.50}Ge_{0.50}I_3$ perovskite-based photovoltaic devices has been carried out. The study highlights the influence of geometric parameters such as the diffusion length of minority carriers and the thickness of the absorber layer on the solar cell performance. A thin ZnO film is used as the transport window layer while a Cu_2O or de NiO film plays the role of buffer layer. The $ZnO(n^+)/Cu_2O(n)/CsSn_{0.50}Ge_{0.50}I_3(p)$ and $ZnO(n^+)/NiO(n)/CsSn_{0.50}Ge_{0.50}I_3(p)$ photovoltaic structures modeled show internal quantum efficiencies of 51.3% and 72.6%, respectively. For the Cu_2O buffer layer, an increase in the internal quantum efficiency from 46.1% to 51.3% and from 45.7% to 52.3% have been observed when varying the $CsSn_{0.50}Ge_{0.50}I_3$ perovskite layer thickness and the minority carrier diffusion length, respectively. For the NiO buffer layer, on the other hand, the quantum efficiency increases from 58.9% to 72.6% for the perovskite layer thickness variation and from 56.2% to 75% for the minority carrier diffusion length variation.

Keywords

Perovskite, Thickness, Diffusion Length, Internal Quantum Efficiency

1. Introduction

Solar cell technologies-based hybrid organic/inorganic perovskite materials have undergone very rapid development. Their photovoltaic conversion efficiency increased from 3.8% in 2009 to 27.3% in 2025 [1] [2]. However, most high-efficiency perovskite solar cells are primarily lead-based [3] [4].

The presence of lead, which is human and environmental highly harmful as well

as the stability issue of these materials, is the major problems encountered in these solar cell technologies. Faced with these difficulties, a large number of lead-free or low-lead content and inorganic alternative perovskites materials have been developed. Theoretically, lead can be replaced by metals such as tin (Sn) [5] [6], bismuth (Bi) [7] [8], copper (Cu) [9], germanium (Ge) [10], or antimony (Sb) [11] [12].

In this work, our attention is focused on the mixed tin-germanium $CsSn_{0.50}Ge_{0.50}I_3$ perovskite absorber. This material exhibits good stability in air and humidity [13], high optical absorption coefficient and a forbidden band gap of 1.5 eV which makes it a good alternative material for photovoltaic applications and other opto-electronic devices.

The influence of buffer layers such as Cu_2O and NiO on the internal quantum efficiency of the $CsSn_{0.50}Ge_{0.50}I_3$ based-solar cell is investigated as well as the thickness and the diffusion length of minority carrier of the base. Cu_2O and NiO thin films allow good electrical contact and the formation of an n-p junction with the $CsSn_{0.50}Ge_{0.50}I_3$ absorber thin film while serving as an interface between the window and active layers.

2. Theoretical Approach and Model

The mathematical equations used to model the operation of the solar cell are those based on the continuity equations of the minority carriers in each part of the solar cell. These continuity equations make it possible to study all the phenomena occurring in semiconductors, to determine the parameters and to better understand the properties of devices made using these materials.

In these calculations, it is assumed that the space charge zone is located between the Cu_2O or de NiO buffer layers (n-type) and $CsSn_{0.50}Ge_{0.50}I_3$ (p-type). The electric field is also assumed to be zero outside this region. In the case of steady state, the continuity equations are given by:

$$\frac{1}{q} div \boldsymbol{J}_n + G_n - R_n = 0$$

$$-\frac{1}{q} div \boldsymbol{J}_p + G_p - R_p = 0$$

In the absence of an electric field, we have:

$$\boldsymbol{J}_n = qD_n \cdot \boldsymbol{grad}\left(n\right)$$

$$\boldsymbol{J}_p = -qD_p \cdot \boldsymbol{grad}\left(p\right)$$

In this work, we limit our calculations to a single dimension and the ZnO(n^+)/Buffer layer(n)/$CsSn_{0.50}Ge_{0.50}I_3$(p) solar cell structure is illustrated in **Figure 1**.

The absorber layer with a band gap energy of 1.5 eV is the $CsSn_{0.50}Ge_{0.50}I_3$ perovskite. It is a p-type semiconductor material whose function is to absorb incident photons from solar radiation in order to generate electron-hole pairs.

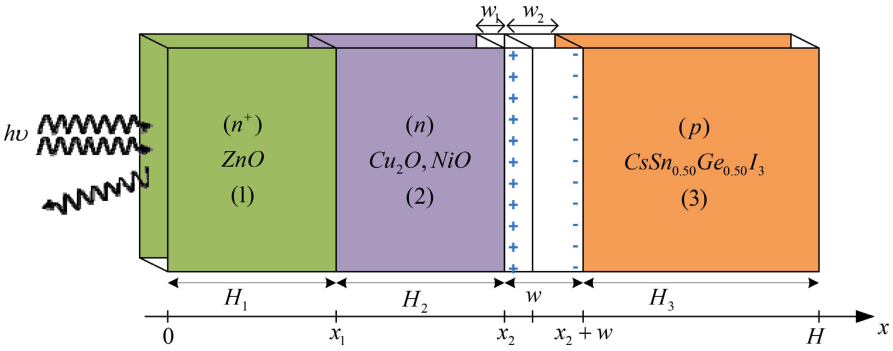

Figure 1. Model of a perovskite solar cell $CsSn_{0.50}Ge_{0.50}I_3$.

The Cu_2O or de NiO a layer of approximately 50 nm thick is deposited on the surface of $CsSn_{0.50}Ge_{0.50}I_3$ film. This n-type semiconductor layer ensures the n-p junction with the absorber and while acting as an interface layer.

The window layer, which is a conductive transparent oxide (ZnO), completes the structure of the solar cell. Its thickness varies between 0.55 mm to 1 mm. It allows incident photons to be transmitted to the absorber and also enables, due to its high conductivity, the collection of charge carriers. It is generally composed of two successive layers. A first intrinsic ZnO layer of about 50 nm thick is used to coat the buffer layer. This is also used to reduce short-circuits. The window layer is then completed by the deposition an aluminum-doped ZnO layer (ZnO:Al), the thickness of which is between 0.5 μm and 1 μm. The highly aluminum-doped ZnO layer exhibits high conductivity and is very transparent, making it then possible for incident photons to pass through to the absorber layer and for charge carriers to be collected.

2.1. Current Density Generated by Light in the Emitter

The hole current density generated by the photons of incident light in the emitter $J_{ph,E}$ includes two contributions: the current density generated in the doped region n^+, J_{ph_1} and the current density generated in the n-doped region, J_{ph_2}

$$J_{ph,E} = J_{ph_1} + J_{ph_2}$$

2.1.1. Current Density Generated in the n^+-Region

The continuity equation in the window layer (ZnO) for minority carriers (the holes) is given by:

$$\frac{\mathrm{d}^2\Delta_{p_1}}{\mathrm{d}x^2} - \frac{\Delta_{p_1}}{L_{p_1}^2} = -\frac{g_{ZnO}}{D_{p_1}}$$

$$g_{ZnO} = \alpha_{ZnO} F\left(1-R\right)\mathrm{e}^{-\alpha_{ZnO}x} \quad \text{And} \quad L_{p_1}^2 = D_{p_1}\tau_{p_1}$$

Δ_{p_1} : Concentration of minority carriers (holes);

L_{p_1} : Diffusion length of holes in the region n^+;

D_{p_1} : Diffusion coefficient of holes in the region n^+;

τ_{p_1} : Lifetime of holes in the region n^+;

α_{ZnO} : Window layer absorption coefficient ZnO;

R : Reflection coefficient;

F : Incident photon flux of energy E and wavelength λ.

The solution of this equation is obtained, taking into account the boundary expressed as followed:

$$D_{p_1}\frac{\partial \Delta_{p_1}}{\partial x} = S_{p_1} \times \Delta_{p_1} \quad \text{For} \quad x = 0$$

$$\Delta_{p_1} = 0 \quad \text{For} \quad x = x_1$$

where S_{p_1} is the recombination rate on the front face of the window layer, J_{ph_1} being the photocurrent in this region is given by:

$$J_{ph_1} = -qD_{p_1}\frac{\partial \Delta_{p_1}(x_1)}{\partial x}$$

$$J_{ph_1} = \frac{q\alpha_{ZnO}F(1-R)L_{p_1}}{\left(\alpha_{ZnO}^2 L_{p_1}^2 - 1\right)} \times \left\{ \frac{\left(\frac{S_{p_1}L_{p_1}}{D_{p_1}} + \alpha_{ZnO}L_{p_1}\right) - e^{-\alpha_{ZnO}x_1}\left[\frac{S_{p_1}L_{p_1}}{D_{p_1}} ch\left(\frac{x_1}{L_{p_1}}\right) + sh\left(\frac{x_1}{L_{p_1}}\right)\right]}{\frac{S_{p_1}L_{p_1}}{D_{p_1}} sh\left(\frac{x_1}{L_{p_1}}\right) + ch\left(\frac{x_1}{L_{p_1}}\right)} - \alpha_{ZnO}L_{p_1}e^{-\alpha_{ZnO}x_1} \right\}$$

2.1.2. Current Density Generated in n-Region

The continuity equation for minority carriers (holes) is given by:

$$\frac{d^2\Delta_{p_2}}{dx^2} - \frac{\Delta_{p_2}}{L_{p_2}^2} = -\frac{g_{BL}}{D_{p_2}}$$

$$g_{BL} = \alpha_{BL}F(1-R)e^{-\alpha_{ZnO}x_1}\cdot e^{-\alpha_{BL}(x-x_1)} \quad \text{and} \quad L_{p_2}^2 = D_{p_2}\tau_{p_2} \quad \text{and}$$

$$BL \equiv \text{Buffer Layer}\left(Cu_2O, NiO\right)$$

L_{p_2} : Diffusion length of holes in region n;

D_{p_2} : Diffusion coefficient of holes in the region n;

τ_{p_2} : Hole lifetime in region n;

α_{BL} : Buffer layer absorption coefficient.

Taking into account the following boundary conditions:

$$D_{p_2}\frac{\partial \Delta_{p_2}}{\partial x} = S_{p_2} \times \Delta_{p_2} + D_{p_1} \times \frac{\partial \Delta_{p_1}}{\partial x} \quad \text{For} \quad x = x_1$$

$$\Delta_{p_2} = 0 \quad \text{For} \quad x = x_2$$

Photovoltaics in the region $x_1 \le x \le x_2$ is given by:

$$J_{ph_2} = -qD_{p_2}\frac{\partial \Delta_{p_2}(x_2)}{\partial x}$$

$$J_{ph_2}=\frac{q\alpha_{BL}F(1-R)L_{p_2}e^{-\alpha_{ZnO}x_1}}{\left(\alpha_2^2L_{p_2}^2-1\right)}$$
$$\times\left\{\frac{\left(\frac{S_{p_2}L_{p_2}}{D_{p_2}}+\alpha_{BL}L_{p_2}\right)-e^{-\alpha_{BL}(x_2-x_1)}\left[\frac{S_{p_2}L_{p_2}}{D_{p_2}}ch\left(\frac{x_2-x_1}{L_{p_2}}\right)+sh\left(\frac{x_2-x_1}{L_{p_2}}\right)\right]}{\frac{S_{p_2}L_{p_2}}{D_{p_2}}sh\left(\frac{x_2-x_1}{L_{p_2}}\right)+ch\left(\frac{x_2-x_1}{L_{p_2}}\right)}-\alpha_{BL}L_{p_2}e^{-\alpha_{BL}(x_2-x_1)}\right\}$$
$$+\frac{J_{ph_1(x_1)}}{\frac{S_{p_2}L_{p_2}}{D_{p_2}}sh\left(\frac{x_2-x_1}{L_{p_2}}\right)+ch\left(\frac{x_2-x_1}{L_{p_2}}\right)}$$

2.2. Current Density Generated in the Space Charge Zone

In the space charge zone, the expression for the current is given by:

$$J_{ZCE}=-qF(1-R)e^{-\alpha_{ZnO}x_1}e^{-\alpha_{BL}(x_2-x_1)}\left[e^{-\alpha_{BL}w_1}-1\right]$$
$$-qF(1-R)e^{-\alpha_{ZnO}x_1}e^{-\alpha_{BL}\left[(x_2+w_1)-x_1\right]}\left[e^{-\alpha_{CsSnGeI}w_2}-1\right]$$

2.3. Current Density Generated in the p-Region

In this region, the photocurrent is an electron due current. The continuity equation for minority carriers (electrons) is given by:

$$\frac{d^2\Delta_{n_3}}{dx^2}-\frac{\Delta_{n_3}}{L_{n_3}^2}=-\frac{g_{CsSnGeI}}{D_{n_3}}$$

$$g_{CsSsGeI}=\alpha_{CsSnGeI}F(1-R)e^{-\alpha_{ZnO}x_1}\cdot e^{-\alpha_{BL}\left[(x_2+w_1)-x_1\right]}\cdot e^{-\alpha_{CsSnGeI}\left[x-(x_2+w_1)\right]}\quad\text{and}\quad L_{n_3}^2=D_{n_3}\tau_{n_3}$$

Δ_{n_3} : Concentration of electrons in the p region;

L_{n_3} : Diffusion length of electrons in the p region;

D_{n_3} : Diffusion coefficient of electrons in the p region;

τ_{n_3} : Lifetimes of electrons in the p region;

$\alpha_{CsSnGeI}$: Absorption coefficient of $CsSn_{0.50}Ge_{0.50}I_3$.

The boundary conditions are given by:

$$D_{n_3}\frac{\partial\Delta_{n_3}}{\partial x}=-S_{n_3}\times\Delta_{n_3}\quad\text{For}\quad x=H$$
$$\Delta_{n_3}=0\quad\text{For}\quad x=x_2+w$$

In this region, the photocurrent is given by:

$$J_{ph_3}=qD_{n_3}\frac{\partial\Delta_{n_3}(x_2+w)}{\partial x}$$

$$J_{ph_3}=-\frac{q\alpha_{CsSnGeI}F(1-R)L_{n_3}e^{-\alpha_{ZnO}x_1}e^{-\alpha_{BL}(x_2-x_1+w_1)}}{\left(\alpha_3^2L_{n_3}^2-1\right)}$$
$$\times\left\{\frac{\left(\alpha_{CsSnGeI}L_{n_3}-\frac{S_{n_3}L_{n_3}}{D_{n_3}}\right)e^{-\alpha_{CsSnGeI}\left[H-(x_2+w_1)\right]}+e^{-\alpha_{CsSnGeI}w_2}\left[\frac{S_{n_3}L_{n_3}}{D_{n_3}}ch\left(\frac{H-(x_2+w)}{L_{n_3}}\right)+sh\left(\frac{H-(x_2+w)}{L_{n_3}}\right)\right]}{\frac{S_{n_3}L_{n_3}}{D_{n_3}}sh\left(\frac{H-(x_2+w)}{L_{n_3}}\right)+ch\left(\frac{H-(x_2+w)}{L_{n_3}}\right)}-\alpha_{CsSnGeI}L_{n_3}e^{-\alpha_{CsSnGeI}w_2}\right\}$$

2.4. Expression of Total Photocurrent

The resulting photocurrent is calculated for each wavelength value. For a given wavelength, it represents, in our model, the sum of all the current components mentioned above, which include the hole diffusion currents in the regions n^+ and n, the current generated in the space charge region and the electron diffusion current in the p-type region.

$$J_{ph,T} = J_{ph,E} + J_{ZCE} + J_{ph_3}$$

The internal quantum efficiency is written as:

$$IQE = \frac{J_{ph,T}}{qF(1-R)}$$

After development of our model and establishment of the equations which govern this latter, we calculated the total current flowing through the solar cell using the absorption coefficients of ZnO, Cu_2O and NiO from the literature [14] [15]. Those of the $CsSn_{0.50}Ge_{0.50}I_3$ perovskite are given by M.S. Alam [13] for photons energies ranging from 0.5 eV to 5 eV.

3. Results and Discussion

Figure 2 highlights the evolution of the internal quantum efficiency of both $ZnO(n^+)/Cu_2O(n)/CsSn_{0.50}Ge_{0.50}I_3(p)$ and $ZnO(n^+)/NiO(n)/CsSn_{0.50}Ge_{0.50}I_3(p)$ photovoltaic devices. In our calculations, the thickness of the $CsSn_{0.50}Ge_{0.50}I_3$ absorber layer and the minority carrier diffusion length in this material are both maintained at 0.5 µm. The carrier diffusion length and the thickness of the ZnO window layer are 0.5 µm and 0.55 µm, respectively. Minority carrier diffusion lengths in both Cu_2O and NiO layers are set at 0.55 µm while the thicknesses of these buffer layers are 0.05 µm.

Figure 2 shows that the maximum conversion efficiencies achieved are 51.3% and 72.6% for Cu_2O and NiO buffer layers, respectively.

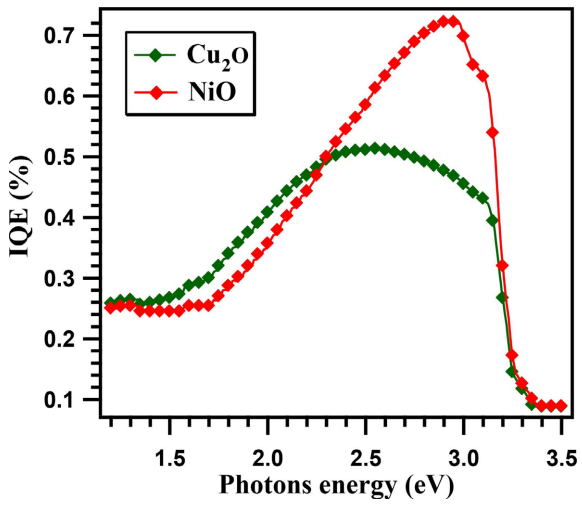

Figure 2. Internal quantum efficiency as a function of energy.

The differences between the quantum efficiencies of the devices can be interpreted from physical mechanisms related to band alignment, optical properties of transport layers and recombination mechanisms.

Indeed, the internal quantum efficiency only becomes important when the absorption coefficient becomes important and when the photogenerated charge carriers can be effectively separated and collected. In both cases, the maximum response observed above the perovskite band gap energy (~1.5 eV) indicates that the collection is better for higher energy photons where optical absorption is higher, carrier generation is closer to the collecting interfaces and therefore carrier diffusion becomes less limiting.

Figure 2 also shows that the nature of the transport layer plays a particularly important role in the internal quantum efficiency of the devices. For the photons with energy close to the perovskite band gap, the absorption is deeper, which increases the recombination risk of the photogenerated carriers.

However, the valence band of Cu_2O, which is better suited to Sn/Ge perovskites than that of NiO, favors a better extraction of the holes at low photon energies (<2.25 eV). This explains the slightly higher internal quantum efficiency observed for the device with Cu_2O in this energy range.

In the device with NiO, the band alignment is less favorable but this range of photon energy (>2.25 eV) is particularly favorable to the generation of carriers close to the collecting interfaces, making the barrier therefore less limiting. This leads to a more efficient collection of the photogenerated carriers, a reduction of the losses by recombination and therefore an improvement of the quantum efficiency in this part of the spectrum.

3.1. Influence of the Thickness and the Minority Carrier Diffusion Length of the Absorber in the Internal Quantum Efficiency

Figure 3 shows the variations of the internal quantum efficiency of devices as a function of the $CsSn_{0.50}Ge_{0.50}I_3$ absorber layer thickness.

The quantum efficiency curves retain the same shapes as those in Figure 2. For the lowest value of the absorber layer thickness, the quantum efficiencies are low and give maximum values of 46.1% and 58.9% for Cu_2O and NiO based devices, respectively.

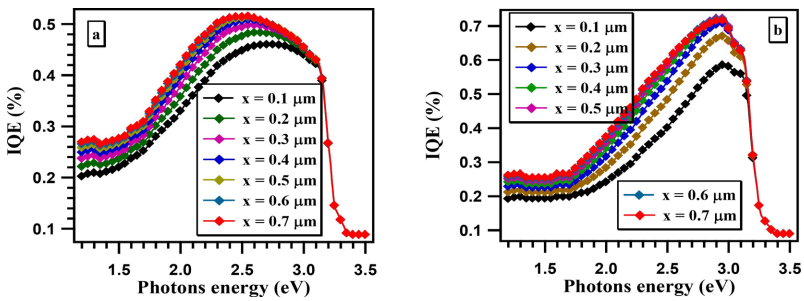

Figure 3. Influence of the absorber layer thickness: (a) in $ZnO(n^+)/Cu_2O(n)/CsSn_{0.50}Ge_{0.50}I_3(p)$; (b) $ZnO(n^+)/NiO(n)/CsSn_{0.50}Ge_{0.50}I_3(p)$ photovoltaic devices.

For both devices, the internal quantum efficiency increases with the absorber layer thickness up to a maximum of 51.5% and 72.8% for $ZnO(n^+)/Cu_2O(n)/CsSn_{0.50}Ge_{0.50}I_3(p)$ and $ZnO(n^+)/NiO(n)/CsSn_{0.50}Ge_{0.50}I_3(p)$, respectively which correspond to an absorber layer thickness of 0.5 µm. Beyond 0.5 µm, our calculations showed that the internal quantum efficiency remains almost constant for both structures as shown in Figure 4.

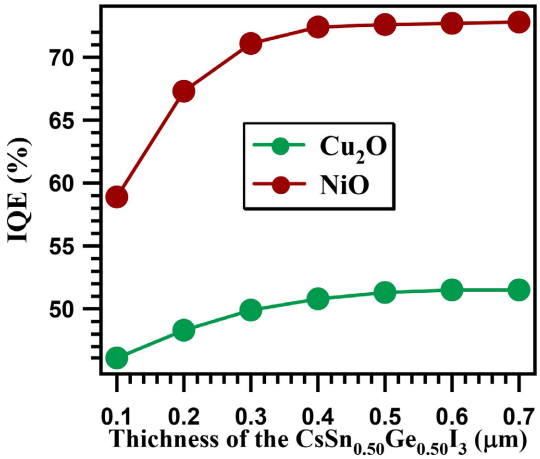

Figure 4. Internal quantum efficiency as a function of the $CsSn_{0.50}Ge_{0.50}I_3$ thickness for the structures $ZnO(n^+)/Cu_2O(n)/CsSn_{0.50}Ge_{0.50}I_3(p)$ and $ZnO(n^+)/NiO(n)/CsSn_{0.50}Ge_{0.50}I_3(p)$.

3.2. Influences of the $CsSn_{0.50}Ge_{0.50}I_3$ Diffusion Length on the Internal Quantum Efficiency

Figure 5 shows the variations of the internal quantum efficiency for different values of the minority carriers diffusion length in the $CsSn_{0.50}Ge_{0.50}I_3$ absorber layer, as a function of photon energy. The diffusion lengths range from 0.1 mm to 0.7 mm.

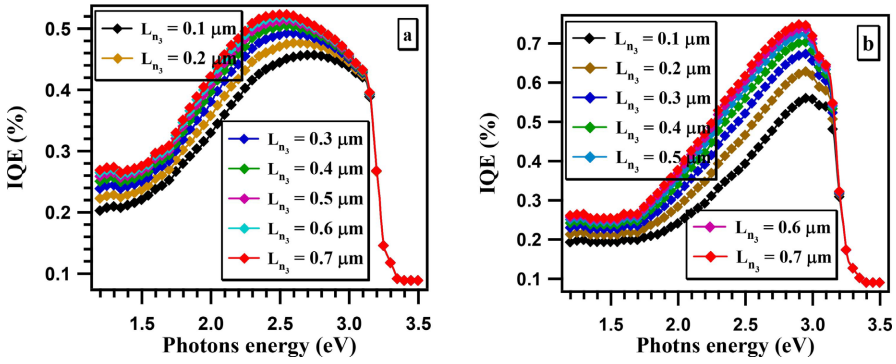

Figure 5. Influence of the minority carrier diffusion length in $CsSn_{0.50}Ge_{0.50}I_3$: (a) $ZnO(n^+)/Cu_2O(n)/CsSn_{0.50}Ge_{0.50}I_3(p)$ and (b) $ZnO(n^+)/NiO(n)/CsSn_{0.50}Ge_{0.50}I_3(p)$.

For both devices, the internal quantum efficiency increases with the diffusion length of the minority carriers in the energy range of 1 eV to 3.1 eV. In this energy

range, photon energies are higher than the band gap energy of the absorber, which allows efficient absorption and carrier generation. The greater diffusion length of the minority carriers, the further they can diffuse and reach the collecting interfaces before recombination, which explains the growth in internal efficiency. Above 3.1 eV, the surface absorption and the optical losses cause a sudden drop in the internal quantum efficiency.

The internal quantum efficiency increases with the minority carrier diffusion length up to a maximum value of 52.3% for the $ZnO(n^+)/Cu_2O(n)/CsSn_{0.50}Ge_{0.50}I_3(p)$ device and up to maximum value of 75%, for the $ZnO(n^+)/NiO(n)/CsSn_{0.50}Ge_{0.50}I_3(p)$ as show in Figure 6.

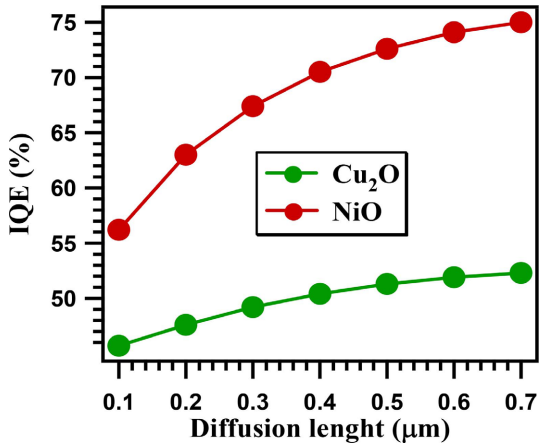

Figure 6. Internal quantum efficiencies as a function of the minority carrier diffusion length in $CsSn_{0.50}Ge_{0.50}I_3$ for $ZnO(n^+)/Cu_2O(n)/CsSn_{0.50}Ge_{0.50}I_3(p)$ and $ZnO(n^+)/NiO(n)/CsSn_{0.50}Ge_{0.50}I_3(p)$ structures.

4. Conclusions

A theoretical investigation of the internal quantum efficiency of photovoltaic devices using the lead-free $CsSn_{0.50}Ge_{0.50}I_3$ perovskite as absorber has been carried out in this work with Cu_2O or NiO used as n-type buffer layer. In both cases, a maximum response is observed above the absorber gap, indicating that the collection is better for higher energy photons.

At low photon energies, the quantum efficiency of the ZnO/Cu_2O architecture is better. For higher photons energies, on the other hand, the combination of a less constraining barrier and a well-adjusted spectral selectivity leads to better transmission and more efficient collection of the photogenerated carriers to give the ZnO/NiO architecture a higher quantum yield with a maximum of 72.6%. The study shows that the thickness of the absorber and the diffusion length of the minority carriers in this layer play a particularly important role in the quantum efficiency of the two devices.

Author Contributions

Saliou Seck: Conceptualization, Data curation, Formal Analysis, Methodology,

Software, Validation, Writing original draft, Writing review & editing;

Alioune Sow: Visualization;

Mamadou Salif Mane: Visualization;

Cheikh Sene: Supervision, Validation, Visualization, Writing review & editing.

All authors have read and agreed to the published version of the manuscript.

Conflicts of Interest

The authors declare no conflicts of interest regarding the publication of this paper.

References

[1] Kojima, A., Teshima, K., Shirai, Y. and Miyasaka, T. (2009) Organometal Halide Perovskites as Visible-Light Sensitizers for Photovoltaic Cells. *Journal of the American Chemical Society*, **131**, 6050-6051. https://doi.org/10.1021/ja809598r

[2] Best Research-Cell Efficiency Chart. https://www.nlr.gov/pv/cell-efficiency

[3] Yin, W., Shi, T. and Yan, Y. (2014) Unique Properties of Halide Perovskites as Possible Origins of the Superior Solar Cell Performance. *Advanced Materials*, **26**, 4653-4658. https://doi.org/10.1002/adma.201306281

[4] Jiang, J., Wang, Q., Jin, Z., Zhang, X., Lei, J., Bin, H., *et al.* (2018) Polymer Doping for High-Efficiency Perovskite Solar Cells with Improved Moisture Stability. *Advanced Energy Materials*, **8**, Article ID: 1701757. https://doi.org/10.1002/aenm.201701757

[5] Kumar, M.H., Dharani, S., Leong, W.L., Boix, P.P., Prabhakar, R.R., Baikie, T., *et al.* (2014) Lead-Free Halide Perovskite Solar Cells with High Photocurrents Realized through Vacancy Modulation. *Advanced Materials*, **26**, 7122-7127. https://doi.org/10.1002/adma.201401991

[6] Cao, D.H., Stoumpos, C.C., Yokoyama, T., Logsdon, J.L., Song, T.-B., Farha, O.K., *et al.* (2017) Thin Films and Solar Cells Based on Semi-Conducting Two-Dimensional Ruddlesden-Popper $(CH_3(CH_2)_3NH_3)_2(CH_3NH_3)_{n-1}Sn_nI_{3n+1}$ Perovskites, *ACS Energy Letters*, **2**, 982-990.

[7] Park, B., Philippe, B., Zhang, X., Rensmo, H., Boschloo, G. and Johansson, E.M.J. (2015) Bismuth Based Hybrid Perovskites $A_3Bi_2I_9$ (A: Methylammonium or Cesium) for Solar Cell Application. *Advanced Materials*, **27**, 6806-6813. https://doi.org/10.1002/adma.201501978

[8] Eckhardt, K., Bon, V., Getzschmann, J., Grothe, J., Wisser, F.M. and Kaskel, S. (2016) Crystallographic Insights into $(CH_3NH_3)_3(Bi_2I_9)$: A New Lead-Free Hybrid Organic–inorganic Material as a Potential Absorber for Photovoltaics. *Chemical Communications*, **52**, 3058-3060. https://doi.org/10.1039/c5cc10455f

[9] Jahandar, M., Heo, J.H., Song, C.E., Kong, K., Shin, W.S., Lee, J., *et al.* (2016) Highly Efficient Metal Halide Substituted $CH_3NH_3I(PbI_2)_{1-x}(CuBr_2)_x$ Planar Perovskite Solar Cells. *Nano Energy*, **27**, 330-339. https://doi.org/10.1016/j.nanoen.2016.07.022

[10] Krishnamoorthy, T., Ding, H., Yan, C., Leong, W.L., Baikie, T., Zhang, Z., *et al.* (2015) Lead-Free Germanium Iodide Perovskite Materials for Photovoltaic Applications. *Journal of Materials Chemistry A*, **3**, 23829-23832. https://doi.org/10.1039/c5ta05741h

[11] Boopathi, K.M., Karuppuswamy, P., Singh, A., Hanmandlu, C., Lin, L., Abbas, S.A., *et al.* (2017) Solution-Processable Antimony-Based Light-Absorbing Materials Beyond Lead Halide Perovskites. *Journal of Materials Chemistry A*, **5**, 20843-20850. https://doi.org/10.1039/c7ta06679a

[12] Zuo, C. and Ding, L. (2017) Lead-Free Perovskite Materials $(NH_4)_3Sb_2I_xBr_{9-x}$. *Angewandte Chemie International Edition*, **56**, 6528-6532. https://doi.org/10.1002/anie.201702265

[13] Alam, M.S., Warda, R.N., Akter, O. and Das, D.K. (2024) Performance Impact of Lead-Free $CsSn_{0.5}Ge_{0.5}I_3$ Based Perovskite Solar Cells with HTL-Free Incorporation. *Global Challenges*, **8**, 5-12. https://doi.org/10.1002/gch2.202400141

[14] Seck, S., Sow, A., Mané, M.S., Ndiaye, A., Keita, E.M., Ndiaye, B., *et al.* (2024) Modeling and Analysis of a Mixed Sn-Ge Lead Free Perovskite Based Solar Cells. *American Journal of Energy Research*, **12**, 1-7.

[15] Seck, S., Sow, A., Mane, M.S., Faye, M., *et al.* (2025) Investigation on Buffer Layers Influence on the Internal Quantum Efficiency of $CH_3NH_3Sn_{(1-y)}Ge_yI_3$ Lead-Free Perovskite-Based Solar Cells. *Advances in Materials*, **14**, 95-104. https://doi.org/10.11648/j.am.20251405.12